



## Conjugated Polymer Blends for Faster Organic Mixed Conductors

Journal:	<i>Materials Horizons</i>
Manuscript ID	MH-COM-07-2022-000861.R1
Article Type:	Communication
Date Submitted by the Author:	21-Oct-2022
Complete List of Authors:	<p>Stingelin, Natalie; Georgia Institute of Technology, ; Imperial College London,            Barker, Micah; University of Bordeaux, LCPO            Nicolini, Tommaso; University of Bordeaux, LCPO            Al Yaman, Yasmina; University of Bordeaux, LCPO            Thuau, Damien; Universite de Bordeaux 1, Institut des Sciences Moléculaires, CNRS UMR5255            Siscan, Olga; University of Bordeaux, LCPO            Ramachandran, Sasikumar; University of Bordeaux, LCPO            Cloutet, Eric; University of Bordeaux, LCPO; CNRS, LCPO            Brochon , Cyril; LCPO            Richter, Lee; National Institute of Standards and Technology, Materials Mesaurment Laboratory            Dautel, Olivier; Charles Gerhardt of Montpellier Institute, AM2N            Hadziioannou, Georges; University of Bordeaux, LCPO</p>

## COMMUNICATION

## Conjugated Polymer Blends for Faster Organic Mixed Conductors

Micah Barker<sup>a</sup>, Tommaso Nicolini<sup>a†</sup>, Yasmina Al Yaman<sup>a</sup>, Damien Thuau<sup>b</sup>, Olga Siscan<sup>a</sup>, Sasikumar Ramachandran<sup>a</sup>, Eric Cloutet<sup>a</sup>, Cyril Brochon<sup>a</sup>, Lee J. Richter<sup>c</sup>, Olivier J. Dautel<sup>d</sup>, Georges Hadziioannou<sup>a\*</sup>, Natalie Stingelin<sup>a,e\*</sup>

Received 00th January 20xx,  
Accepted 00th January 20xx

DOI: 10.1039/x0xx00000x

**A model mixed-conducting polymer, blended with an amphiphilic block-copolymer, is shown to yield systems with drastically enhanced electrochemical doping kinetics, leading to faster electrochemical transistors with a high transduction. Importantly, this approach is robust and reproducible, and should be readily adaptable to other mixed conductors without the need for exhaustive chemical modification.**

**New Concepts:** Semiconducting polymers attract great interest for bioelectronics applications due to their soft nature and mixed ionic-electronic conduction capabilities. So far, most efforts focused on enhancing mixed-conducting functionalities by introducing polar side chains. Here, we show that blending offers a powerful, general approach to improve mixed conduction. We used a block copolymer of poly(3-hexylthiophene) and poly(ethylene oxide) (P3HT-b-PEO) as additive for a relatively poorly performing model material based on a random copolymer between 3-hexylthiophene and 3-(6-hydroxy)hexylthiophene, (P(3HT-co-3HHT)), to unambiguously demonstrate the benefit of our strategy. Blends and neat P(3HT-co-3HHT) show similar transduction performance when implemented in organic electrochemical transistors (OECT)s, yet, intriguingly, blends display drastically reduced drain-current hysteresis because of faster electrochemical doping; i.e., blending introduces ion-transporting pathways without negatively affecting the semiconductor's electronic conductivity. This is desired for electrochemical transducer operation and is rendered possible via use of the amphiphilic block copolymer that imparts the required hydrophilicity to the active layer and promotes partial miscibility between active-layer components without the need of stabilizing the films by cross-linking. Additionally, a notable threshold-voltage stability across gate-potential sweep rates and a low impedance is found, thanks to the electrolyte/redox-polymer compatibilization due to the presence of the additive, rendering these blends promising for numerous applications, including electrochemical biosensing.

<sup>a</sup>Université de Bordeaux, CNRS Bordeaux INP/ENSCBP, Laboratoire de Chimie des Polymères Organiques, UMR 5629, Allée Geoffroy Saint-Hilaire, 33615 Pessac Cedex, France

<sup>b</sup>Université de Bordeaux, CNRS Bordeaux INP/ENSCBP Laboratoire de l'Intégration du Matériau au Système UMR 5218, 16 Avenue Pey Berland, 33607 Pessac Cedex, France

<sup>c</sup>Material Measurement Laboratory, National Institute of Standards and Technology, Gaithersburg, Maryland 20899, USA

<sup>d</sup>Institut Charles Gerhardt Montpellier, UMR 5253 CNRS-UM-ENSCM. Campus CNRS-Bâtiment Balard, 1919, route de Mende, 34293 Montpellier Cedex 05, France

<sup>e</sup>School of Materials Science & Engineering and School of Chemical & Biomolecular Engineering, Georgia Institute of Technology, Atlanta, GA 30332, USA

\*Email: natalie.stingelin@gatech.edu; georges.hadziioannou@u-bordeaux.fr;

Keywords: Organic mixed ionic/electronic conductors, semiconducting polymer blends, organic electrochemical transistors (OECTs)

## Introduction

The growth of the organic bioelectronics field over the past two decades has been rapid, driven by the potential of semiconducting polymers to impact future medical technology platforms, neuromorphic sensor systems, batteries, and beyond.<sup>1</sup> Among the most beneficial features of the versatile materials class of 'plastic' semiconductors are their unique, tunable electrochemical characteristics and the possibility to introduce mixed ionic and electronic conducting properties that, combined, lead to bulk doping and/or de-doping in the presence of electrolytes and may be exploited in applications where transduction between biochemical ionic fluxes and electronics is required. Specifically, electrochemical oxidation of the polymers' conjugated backbone will modulate their electrical conductivity and can produce large volumetric capacitances ( $C^*$ ) – effects that, combined, can result in high signal amplification when integrated in devices such as biosensors.<sup>2,31</sup> However, critical processes leading to mixed conduction<sup>32</sup> rely on ion transport across polymer/analyte interfaces as well as through the bulk of the polymer structure, both of which can limit the response speed of devices such as organic electrochemical transistors (OECTs).<sup>3</sup> One common strategy to support ion transport in polymeric semiconductors<sup>33</sup> involves chemically engineering the polarity of the materials' side chains by introducing, e.g., organic acid or ionic groups, and/or using oligo(ethylene glycol) side chains,<sup>4-8</sup> which all lead to mixed-conduction, bulk electrochemical doping, and high volumetric capacitances. To date, use of oligo(ethylene glycol) side chains has resulted in the highest augmentation of  $C^*$ , enabling a high steady-state transduction performance in OECTs (cf. Ref. 8). The choice of backbone chemistry, in addition, offers access to depletion, accumulation, or ambipolar modes of OECT operation, thereby, providing a plethora of options for materials design and having resulted in a steady growth of the polymer mixed conductor library.<sup>4-8</sup>

There are, however, limitations when using a single-component material for OECT applications. For example, because of the required polar side-chain functionalization, the polymers often become water soluble, resulting in the need for cross-linking the material post film deposition and/or for the use of slowly diffusing bulky counter-ions to be compatible with applications in aqueous media.<sup>5</sup> Significant water uptake –passive or during operation– can bring about irreversible morphological changes in the material's solid-state structure, often with drastic consequences on their electronic function and device stability,<sup>9</sup> in many cases combined with a pronounced sensitivity to humidity.<sup>9,10</sup> Furthermore, bulky side groups can lead to torsional backbone disorder which can detrimentally affect electronic charge-carrier mobility.<sup>11,12</sup> The interplay of these effects is typically not predictable; accordingly, a series of polymers generally needs to be synthesized, typically exploiting

co-polymerization and variation of the side-chain substitution pattern, to understand and fine-tune materials performance.<sup>13-15</sup>

Alternatively, multicomponent systems may be used to introduce specific functionalities via blending together different materials, without the need for complex chemical designs of the active semiconductor polymer itself.<sup>16,17</sup> For instance, in the organic thin-film transistor field, addition of the bulk commodity polymer, polyethylene, to a polymer semiconductor has resulted in structures of increased mechanical robustness, enhanced environmental stability, smaller gate-bias stress and, in many cases, improved electron and hole transport, even at very high content of the insulating 'additive'.<sup>16,18,19</sup> Transport was also maintained in the bulk,<sup>20</sup> allowing fabrication of organic solar cells using a donor polymer, acceptor fullerene derivative and polyethylene ternary blend.<sup>21</sup> Here, we show that a similar approach can be employed for enhancing the electronic/ionic mixed conduction properties of polymeric semiconductors. In contrast to thin-film transistors, however, where highly apolar additives need to be employed that are inactive and are incompatible with the semiconductor<sup>18</sup>, for OECTs, where bulk doping/charge transport is required, an amphiphilic additive needs to be used that can simultaneously enhance the overall hydrophilicity and ionic conductivity of the system, while keeping the active layer water-insoluble without requiring a cross-linking agent and without affecting the molecular packing of the semiconductor, critical for electronic transport.

## Results and discussion

We selected as model mixed conductor a random copolymer based on the archetypal polymer semiconductor poly(3-hexylthiophene) (P3HT) and resulting from the copolymerization of 3-hexylthiophene (3HT) and 3-(6-hydroxy)hexylthiophene (3HHT), *i.e.* P(3HT-*co*-3HHT) (50:50 mol ratio of 3HT:3HHT; number-average molecular mass,  $M_n = 30 \text{ kg mol}^{-1}$ , dispersity  $\bar{D} = 1.9$ ). We chose a material with this particular conjugated backbone because these polymers are known to have somewhat limited hole mobilities with respect to other state of the art organic mixed conductors<sup>24</sup> thus can serve as an excellent model system to demonstrate the efficacy – and generality – of blending to enhance ion transport in OECT active layers. We like to also note that for this mixed conductor, it was previously shown that the hydroxyhexyl (-C<sub>6</sub>H<sub>12</sub>OH) side chains in the 3HHT moieties can enhance its electrochemical response in aqueous media,<sup>22,23</sup> while not affecting the molecular order and the electronic/ionic properties of solution-cast films even after OECT device operation.

To produce a multicomponent system of desired function, we blended the P(3HT-*co*-3HHT) with a block-copolymer of P3HT and ion-conducting poly(ethylene oxide) (P3HT-*b*-PEO;  $M_{n, \text{P3HT}} = 5 \text{ kg mol}^{-1}$ ,  $M_{n, \text{PEO}} = 20 \text{ kg mol}^{-1}$ ). We used a block copolymer rather than a PEO homopolymer to limit phase separation when combined with the more apolar P(3HT-*co*-3HHT). An additional benefit of using a block-copolymer is that this component still provides sites within the P3HT block that can be electrochemically oxidized, thus, potentially minimizing impact on the volumetric capacitance of the system. The chemical structures of the polymers are shown in the insets of **Figure 1a**.

Blend films could be readily prepared via spin-coating from a co-solvent—a 1:1 mixture (by volume fraction) of tetrahydrofuran (THF) and N-methylpyrrolidone (NMP)—using a concentration of  $15 \text{ mg mL}^{-1}$ , followed by drying at  $55 \text{ }^\circ\text{C}$  for (3 to 8) min and subsequent exposure to dynamic vacuum overnight to extract excess NMP. Reassuringly, no large scale phase separation was observed in optical microscopy, although distinct features for P(3HT-*co*-3HHT) and the PEO-block in P3HT-*b*-PEO were observed both in grazing-incidence wide-angle X-ray

scattering (GIWAXS) and differential scanning calorimetry (DSC), see Figure S3 to S5. [Note, no melting endotherm was found for the P3HT-blocks in neat P3HT-*b*-PEO suggesting that they are of relatively low molecular order]. Moreover, the water contact angle notably decreases upon addition of P3HT-*b*-PEO to P(3HT-*co*-3HHT) (Figure S6), from which we infer that the block-copolymer increases at least the surface polarity of the system.

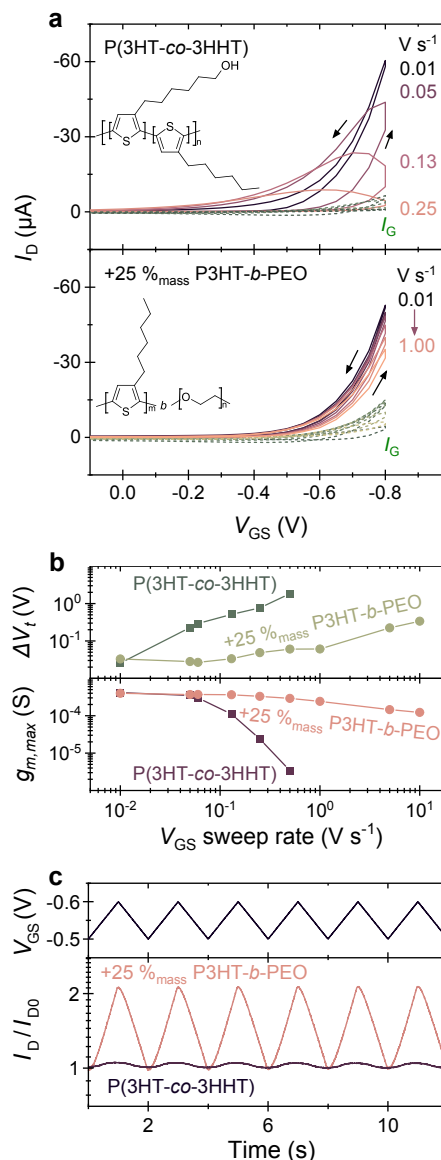


**Figure 1.** a) OECT transfer curves of P(3HT-*co*-3HHT) (left) and its blend with P3HT-*b*-PEO (right) measured by cyclic application of Gate-Source voltage ( $V_{GS}$ ) at indicated sweep rates and constant Drain-Source voltage ( $V_{DS} = -0.6 \text{ V}$ ), showing less hysteresis in current traces upon blending. The chemical structures of the components are shown in the inset. b) Threshold voltage difference between forward and reverse scans ( $\Delta V_t$ ) (top) and maximum transconductance during forward scans ( $g_{m, \text{max}}$ ) (bottom) extracted from data in (a). c) OECT transient drain currents in response to the indicated  $V_{GS}$  waveform (measured at  $V_{DS} = -0.4 \text{ V}$ ). Results obtained from devices of similar channel dimensions (width  $W = 100 \text{ } \mu\text{m}$ , length  $L = 10 \text{ } \mu\text{m}$ , and thickness  $d = 110 \text{ nm}$ ) using  $0.1 \text{ mol L}^{-1}$  KCl aqueous electrolyte.

Films of thicknesses of (80 to 200) nm were used to fabricate OECTs, following procedures detailed in the Supplementary Information. The OECTs were operated in an aqueous solution of  $0.1 \text{ mol L}^{-1}$  KCl, and the drain current ( $I_D$ ) response to cyclic application of a Gate-Source potential ( $V_{GS}$ ) from 0.2 to -0.8 V in -0.05 V increments was measured at various Gate-Source voltage sweep rates and at a constant Drain-Source

voltage ( $V_{DS}$ ) of  $-0.6$  V. The resulting transfer characteristics ( $I_D$  vs.  $V_{GS}$ ) for P(3HT-*co*-3HHT) and a blend of P(3HT-*co*-3HHT) with 25 %<sub>mass</sub> ratio (hereafter %<sub>mass</sub>) of P3HT-*b*-PEO are displayed in **Figure 1a**. Schematics of the device architecture used, transfer curve of the blend device with 25 %<sub>mass</sub> P3HT-*b*-PEO, with  $I_{DS}$  plotted on a logarithmic scale, and data for other blend compositions, (10, 33, 40, and 45) %<sub>mass</sub> P3HT-*b*-PEO, are shown in Figure S7. Corresponding output characteristics for the neat P(3HT-*co*-3HHT) and the 75:25 (by mass) P(3HT-*co*-3HHT):P3HT-*b*-PEO blends are displayed in Figure S8.

Immediately apparent is that OECTs comprising the neat P(3HT-*co*-3HHT) as channel material display a pronounced hysteresis, especially at faster operation. Gate-Source voltage sweep rates as low as  $0.01$   $V$   $s^{-1}$  were needed to minimize the observed hysteresis and attain reasonable drain currents ( $\approx 60$   $\mu A$ ) for a transistor with a channel width,  $W$ , of  $100$   $\mu m$ , a channel length,  $L$ , of  $10$   $\mu m$ , and an active layer thickness,  $d$ , of  $110$  nm. In strong contrast, in 75:25 P(3HT-*co*-3HHT):P3HT-*b*-PEO blends, a minimal hysteresis is observed even at sweep rates up to  $1$   $V$   $s^{-1}$ , while reaching drain currents of (30 to 60)  $\mu A$ , leading to a current modulation of 100 to 500 (Figure S7).

The different behavior of the blend vs. the neat P(3HT-*co*-3HHT) can be better illustrated by plotting the extrapolated threshold voltage shifts between the forward and reverse scans ( $\Delta V_t$ ), see **Figure 1b**, top panel (further details are given in Figures S7). At a Gate-Source voltage sweep rate of  $0.01$   $V$   $s^{-1}$ , the lowest rate used in this work,  $\Delta V_t$  extracted for both systems are comparable,  $\approx (20$  to  $30)$  mV. However, increasing the sweep rate to  $0.1$   $V$   $s^{-1}$  leads to a notable increase of  $\Delta V_t$  by an order of magnitude for neat P(3HT-*co*-3HHT), reaching  $\geq 1$  V at sweep rates of  $0.1$   $V$   $s^{-1}$  and higher (see also Figure S10). In devices of the 75:25 blend, conversely, a low  $\Delta V_t$  of (20 to 50) mV was maintained even when the OECT was operated at sweep rates of  $1$   $V$   $s^{-1}$ . Remarkably, even at  $10$   $V$   $s^{-1}$ , the increase of  $\Delta V_t$  in the blends is smaller than that observed in devices of the neat material when operated at a rate of  $1$   $V$   $s^{-1}$ , *i.e.*, one order of magnitude slower. Data for a broader range of blend compositions are shown in Figure S11.

A similar observation can be made for the transconductance,  $g_m$ , an important OECT figure-of-merit that is directly related to the hole mobility ( $\mu$ ),  $C^*$ , and device relevant parameters and dimensions including  $V_t$ ,  $V_{GS}$ ,  $W$ ,  $L$  and  $d$ , via the following equation:<sup>2</sup>

$$g_m = \mu C^* (|V_t - V_{GS}|)(Wd/L)$$

As **Figure 1b**, bottom panel, shows, at slow Gate-Source voltage sweeps, the maximum transconductance,  $g_{m,max}$  is comparable for the neat and blended systems, but  $g_{m,max}$  distinctly diverges when higher sweep rates are used, with  $g_{m,max}$  rapidly decreasing for neat P(3HT-*co*-3HHT) for rates  $> 10^{-1}$   $V$   $s^{-1}$ , while for the 75:25 blend it stayed relatively constant (around  $0.4$  mS) over the entire Gate-Source voltage sweep rate range tested, (0.1 to  $10$ )  $V$   $s^{-1}$ . [Note: Figure S9 illustrates how  $g_{m,max}$  and  $\Delta V_t$  were deduced].

The consistency in performance of blend devices is further highlighted by comparing devices of a range of geometries (*i.e.*, different channel dimensions; **Figure 2a,b**), where we consistently observe for the 75:25 P(3HT-*co*-3HHT):P3HT-*b*-PEO a transconductance,  $g_m$ , that scales with OECT dimensions, typically given as  $|V_t - V_{GS}| (WdL^{-1})$ ,<sup>24</sup> starkly contrasting with the neat copolymer, for which a large dispersion in  $g_m$  is found across Gate-Source voltage sweep rates, especially at low  $|V_t - V_{GS}| (WdL^{-1})$  values.

From the slope of  $g_m$  vs.  $|V_t - V_{GS}| (WdL^{-1})$ , we can deduce  $\mu C^*$ , indicated in **Figure 2a,b** with a dashed line. Intriguingly,  $\mu C^*$  for the 75:25 blend ( $\approx 25$   $F$   $cm^{-1} V^{-1} s^{-1}$  across sweep rates;  $\pm 3$   $F$   $cm^{-1} V^{-1} s^{-1}$  standard deviation) converges with the range of  $\mu C^*$  that can be deduced for the neat P(3HT-*co*-3HHT) across sweep rates investigated

here ( $\approx 36$   $F$   $cm^{-1} V^{-1} s^{-1}$ ;  $\pm 20$   $F$   $cm^{-1} V^{-1} s^{-1}$  standard deviation). This observation suggests that introduction of the block-copolymer at this content (25 %<sub>mass</sub> P3HT-*b*-PEO) does not strongly affect  $\mu C^*$ , which implies that either  $\mu$  or  $C^*$  increases while  $C^*$  or  $\mu$  is decreasing, or  $\mu C^*$  stays constant.

The importance of reaching maximum transconductance over a wider range of times scales for, *e.g.*, the blend with 25 %<sub>mass</sub> P3HT-*b*-PEO with respect to the neat material becomes clear from the transient measurements displayed in **Figure 1c**. The triangular waveform applied at the gate is transduced to a significant  $I_D$ -modulation only for the blend comprising 25 %<sub>mass</sub> P3HT-*b*-PEO. Increasing the block-copolymer fraction above 25 %<sub>mass</sub>, does however reduce  $\mu C^*$ , especially at contents of  $\geq 40$  %<sub>mass</sub> P3HT-*b*-PEO. Accordingly, blend compositions can be identified where a compromise is reached where  $\Delta V_t$  is sufficiently low while  $\mu C^*$  remains relatively high. Comparing the top panel with the bottom panel of **Figure 2c**, this is reached for a block-copolymer content between (20 to 40) %<sub>mass</sub> (see also Figure S12).

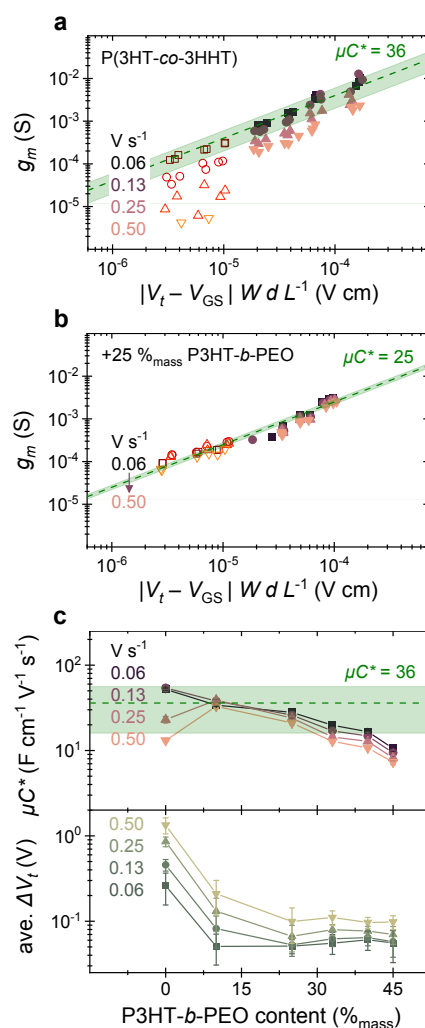


Figure 2. OECT Transconductance ( $g_m$ ) plotted against the product of Gate-Source bias and channel dimensions ( $|V_t - V_{GS}| W d L^{-1}$ ) for several devices with a) P(3HT-*co*-3HHT) and b) 25 %<sub>mass</sub> P3HT-*b*-PEO as channel material. Data from devices with micro-scale Source and Drain electrodes patterned by photolithography are shown in red gradient (open symbols), while those of large-scale devices are shown in pink gradient (solid symbols). Data for other blend compositions are shown in Figure S12. c) Summary of  $\mu C^*$  (top) and average Gate threshold voltage difference (ave.  $\Delta V_t$ ) (bottom) extracted for various blend compositions at indicated scan rates. Error bars represent sample standard deviation of at least 12 devices. Green dashed line and shaded regions indicate average  $\mu C^*$  in units of  $F$   $cm^{-1} V^{-1} s^{-1}$  and its standard deviation, respectively, measured across sweep rates for the neat P(3HT-*co*-3HHT) in a) and c), and for the 25 %<sub>mass</sub> blend in b).

In order to gain a more mechanistic understanding of  $\mu \cdot C^*$  upon blending, we analyzed various blends with electrochemical impedance spectroscopy (EIS) and compared these with the neat P(3HT-co-3HHT). The impedance magnitude ( $|Z|$ ) and the corresponding Nyquist ( $Z_{im}$  vs  $Z_{re}$ ) plots are displayed in **Figure 3a,b**, respectively. A few observations can be immediately made. In the high ( $>10^3$  Hz) and low ( $<1$  Hz) frequency range, the behavior with respect to  $|Z|$  of blends and the neat co-polymer are comparable, while addition of P3HT-*b*-PEO to P(3HT-co-3HHT) clearly depresses  $|Z|$  in the mid-frequency regime, (1 to  $10^3$ ) Hz.

This behavior can be modelled with a second-order Voigt-type equivalent circuit (Figure 3a, inset), typically used in simplified models of Li-ion battery and supercapacitor cells<sup>25,26</sup> and consisting of three elements: a resistance ( $R_S$ ) resulting from the solution/electrolyte resistance and dominating the high frequency regime; a capacitor ( $C_p$ ) in parallel with a resistor ( $R_p$ ) that we ascribe to the low frequency range and can be assigned to the capacitance and resistance of the polymer film (neat or blended); and a constant phase element (CPE) in parallel with a resistor ( $R_{CT}$ ) that we used to describe the mid-frequency behavior, which we attribute to inhomogeneous double layer capacitive charging<sup>27</sup> and ion injection occurring at the polymer/electrolyte interface. Since  $|Z|$  decreases in this mid-frequency regime, indicating a lowering of ion injection resistance upon addition of the block-copolymer, we conclude that the PEO-block assists in 'blurring' the interfaces between the polymer layer and the electrolyte. This is likely due to the increased polarity of such blends, as deduced from the decrease of the water contact angles from  $96^\circ$  for the neat P(3HT-co-3HHT) to  $72^\circ$  for the blended film with 45 %mass P3HT-*b*-PEO (Figure S6), combined possibly with an enhanced ion transport due to the addition of the polar PEO moiety. This behavior is illustrated in the Nyquist plots, where blending minimizes the depressed semi-circle feature, converging at around 45 %mass P3HT-*b*-PEO content. Parameters extracted for the various blends are listed in Table S1, and a plot at low impedance values is shown in Figure S13.

Importantly, because the equivalent circuit that we used for modelling the impedance spectra is approaching that of a simple Randle cell of [ $R_S$  ( $C_p || R_p$ )], average  $C^*$  can be deduced for the various systems from the capacitance values  $C_p$  in the low-frequency regime (the capacitor component in parallel with  $R_p$ ) for films of a range of thicknesses (Table S1). The results are summarized in **Figure 3c**. Relatively small variations in  $C^*$  ( $\approx 190 \text{ F cm}^{-3}$ ;  $\pm 20 \text{ F cm}^{-3}$  standard deviation; measured at a DC offset of 0.75 V) are extracted for neat P(3HT-co-3HHT) and its blends with P3HT-*b*-PEO independent of block-copolymer content. Considering that  $\mu \cdot C^*$  is of the order of  $10^1 \text{ F cm}^{-1} \text{ V}^{-1} \text{ s}^{-1}$ , we estimate a hole mobility of the order of  $\approx 10^{-1} \text{ cm}^2 \text{ V}^{-1} \text{ s}^{-1}$ , which is in accordance with literature on such side-chain-functionalized thiophene-based mixed conducting materials<sup>23,28</sup>.

The finding that  $\mu \cdot C^*$  is essentially constant over a large blend composition range is somewhat surprising, but may give some insights on the blends' phase behavior, considering that  $C^*$  describes the strength of the ionic-electronic coupling in a material and is related to the charge-carrier density.<sup>2,3,24,29</sup> Specifically, the fact that  $C^*$  is unaffected by the addition of the block-copolymer suggests that addition of the PEO-block does not reduce the amount of charge carriers that can be induced upon electrochemical doping.

We infer from this finding that in the blends similar amounts of 3HT- and 3HHT-segments are available that can be oxidized as in the neat P(3HT-co-3HHT). Since the crystalline regions in P(3HT-co-3HHT) seem not to drastically swell upon exposure to humidity (see Figure S14) and thus, likely, exposure to an electrolyte, we speculate that the amorphous regions in the thin-film structures are regulating the injection and transport of ions during application of a bias on the

polymer film. Since these ions are necessary to balance the positive charge of polarons in the electroactive material, we attribute to the amorphous fractions a key role in determining the kinetics and electrochemical doping efficiency. In this context, it is important to note that blending leads to a certain degree of vitrification of both components. We infer this from DSC measurements, extracting the enthalpy values for the P(3HT-co-3HHT)/P3HT and PEO-block melting endotherms at  $\approx 245^\circ \text{C}$  and  $\approx 50^\circ \text{C}$ , *i.e.*  $\Delta H_{3\text{HT}/3\text{HHT}}$  and  $\Delta H_{\text{PEO}}$  respectively (Figure S5, bottom panel). The solid lines show the enthalpy values for the two moieties (3HT/3HHT vs. PEO) while the corresponding dashed lines describe the "ideal" values (the expected enthalpies in case the materials would fully phase separate and no interactions between the components occurs); *i.e.*, a scenario where both P(3HT-co-3HHT) and P3HT-*b*-PEO can crystallize essentially as unhindered as in the neat form. Enthalpy values below this ideal line as observed here, therefore, indicate that blending suppresses crystallization of the specific moiety/block, leading to a higher molecular disorder in the blend as compared to the neat films. A positive deviation, *vice versa*, would suggest that blending of the materials promotes the crystallization of one or both components.

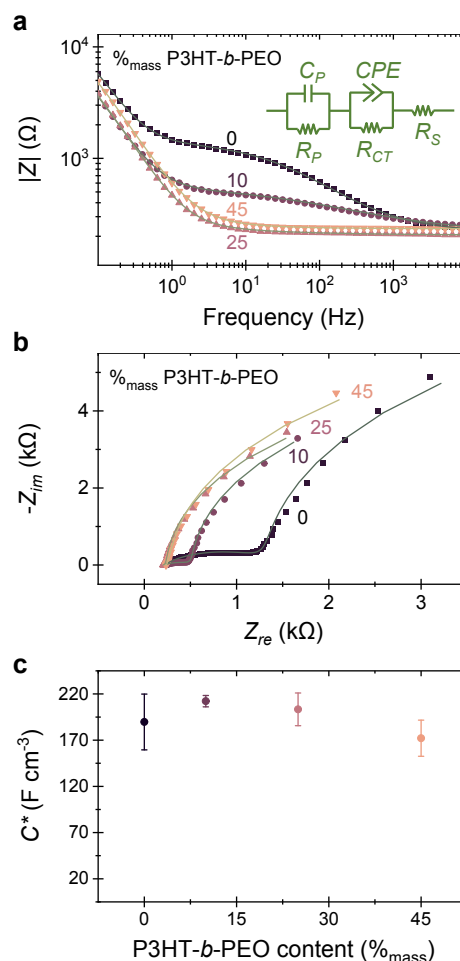


**Figure 3.** a) Bode plots ( $|Z|$  vs  $f$ ) and b) Nyquist plots ( $Z_{im}$  vs  $Z_{re}$ ) measured for P(3HT-co-3HHT) and its blends with P3HT-*b*-PEO. Experimental data (scatter plots) could be modelled reasonably well with the equivalent circuit shown in (a) (solid lines). [Note: a constant phase element (CPE) was used instead of an ideal capacitor element to better fit the experiment data.] c) Volumetric capacitance ( $C^*$ ) calculated using CP extracted from model fits to experimental data for films of various thickness and blend compositions, showing similar values. Error bars represent standard deviation of at least 3 samples.

Since addition of P3HT-*b*-PEO to P(3HT-*co*-3HHT) results in a larger fraction of amorphous phase, we conclude that blending does not reduce the amounts of segments available that can be oxidized but, rather, increases them. This effect counter-acts the reduction in overall active material through introduction of the PEO block. Hence, a compromise can be found where the polarity of a system is increased, and ion transport be enhanced, without negatively impacting  $C^*$ . This results in drastically faster response times when such blends are implemented in OECTs, promising devices of higher sensitivity and signal amplification, as illustrated by the OECT time constants ( $\tau$ ) extracted from the transient drain currents in response to an applied Gate-Source bias (Figure S15). While  $\tau$  for the neat material is around 8 s, for the 75:25 blends a time constant of 80 ms is found. Consequently, blend devices exhibit significantly larger output current amplitudes than those of the neat material upon application of a moderate Gate-Source bias wave-period signal (triangle wave, period  $T = 2$  s), as shown in Figure 1c.

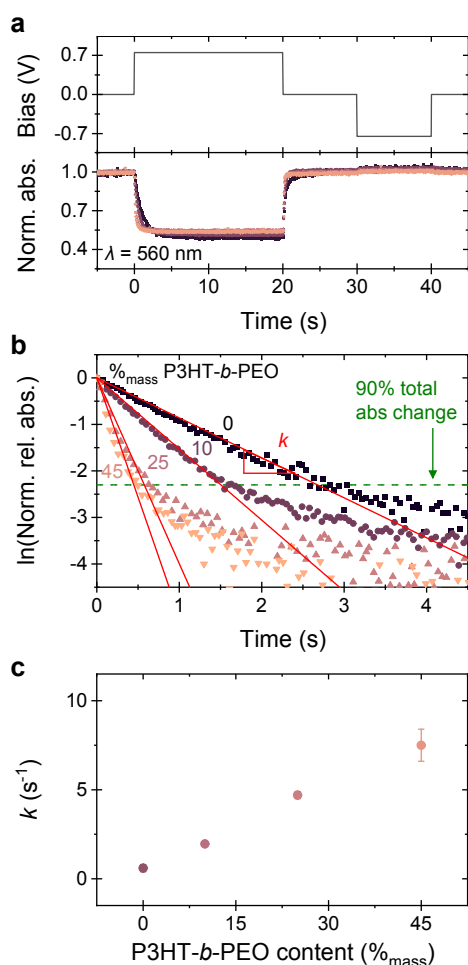


**Figure 4.** a) Absorbance changes during application of potential on a polymer/ITO electrode (0.75 V vs. Ag/AgCl wire) in 0.1 mol L<sup>-1</sup> KCl, showing similar intensity decrease for blends with (0 to 45) %<sub>mass</sub> P3HT-*b*-PEO. b) Logarithmic plot of relative absorbance over time, showing faster decrease with higher P3HT-*b*-PEO content. c) Rate constants ( $k$ ) extracted from (b) plotted against corresponding blend composition. Results obtained from films of similar thickness ( $d = 110 \pm 10$  nm). Error bars represent standard deviation of at least 3 measurements.

Spectroelectrochemical data of the blends cast on indium tin oxide (ITO) electrodes support the view that the observed transient OECT behavior can be attributed to faster electrochemical doping of the semiconducting layer upon addition of P3HT-*b*-PEO (Figure 4; details are given in the SI). In the neutral state, blends of different P3HT-*b*-PEO

content of (0 to 45) %<sub>mass</sub> show essentially identical absorption with a maxima at 560 nm and only slight differences in the 0-1/0-0 vibronic peak ratios (Figure S16).<sup>10</sup> Application of a potential at the polymer/ITO electrode (0.75 V vs an Ag/AgCl wire electrode in 0.1 mol L<sup>-1</sup> KCl, chosen based on the cyclic voltammetry data shown in Figure S17) results in a decrease of this ground-state absorption band for all blend compositions, accompanied by an increase of a broad polaron absorption<sup>30</sup> at longer wavelengths (Figure S18). This process is typically reversible if a 0 V bias is applied between the polymer film and the Ag/AgCl wire electrode in a subsequent step. Furthermore, no significant degradation of the doping kinetics nor the extent of doping was observed up to 10 doping/de-doping cycles for the blend with 25 %<sub>mass</sub> P3HT-*b*-PEO as compared to the neat material (Figure S19).

The dynamics of the electrochemical doping/de-doping can be visualized by plotting the normalized absorbance as function of time and applied bias<sup>22,30</sup> (Figure 4a) for the different blends/neat P(3HT-*co*-3HHT). An evident, faster response is observed for the blends (pink to purple traces) compared to the neat P(3HT-*co*-3HHT) (black trace), with blends of higher P3HT-*b*-PEO content (light pink traces) displaying the fastest response. Moreover, only small differences between the normalized absorbance at saturation (at 0.75 V vs an Ag/AgCl wire) are found between the blends and the neat P(3HT-*co*-3HHT), emphasizing that they can be electrochemically equally doped; *i.e.*, equal amounts of charges are introduced, in agreement with the similar  $C^*$  values we extract for all systems.

Closer inspection of the optical response within the first few seconds of applying a potential and using the normalized relative absorbance (Figure 4b; further details are given in Figure S18) allows us to extract the electrochemical doping rate constants ( $k$ ) from exponential decay fits of the data, assuming that the change in absorbance is directly proportional to the decrease of neutral 3HT or 3HHT segments and follows first order kinetics. A single-phase exponential decay function fits adequately with the experimental data until about 90 % of the total absorbance change (green dotted line in Figure 4b, Figure S18), after which the signal slowly saturates. Plotting the extracted rate constants,  $k$ , it is immediately apparent that increasing the P3HT-*b*-PEO content in the blends results in drastically higher  $k$  (Figure 4c), further highlighting that introduction of the block-copolymer to the P(3HT-*co*-3HHT) assists ion transport in the system. Additionally,  $k$  is thickness dependent (Figure S18d, e, f), from which we conclude that the electrochemical doping/de-doping is a bulk process.

## Conclusions

Our work shows that blending can be an effective strategy to enhance the transient performance of polymeric mixed conductors without the need for significant chemical modification. Adding P3HT-*b*-PEO to the mixed conducting P(3HT-*co*-3HHT) supports faster electrochemical doping of the system in aqueous media, enhancing in turn the response speed of OECT devices. Tellingly, our approach works even for relatively non-polar semiconductors, such as the prototypical P3HT. The electrochemical spectroscopy and OECT data shown in Figure S20 and S21 illustrate that blends of 75:25 P3HT: P3HT-*b*-PEO operate rather cleanly in an aqueous electrolyte, in stark contrast to neat P3HT. Indeed, no amplification of the source-drain current is observed for neat P3HT OECTs, while in blends, clear transistor behavior is recorded.

We attribute the beneficial effect of blending with the block-copolymer to an increase in hydrophilicity of blend thin-film structures introduced by the presence of the PEO moieties. This seems to assist in enhancing the compatibility between the active blend film and the aqueous electrolyte, effectively 'blurring'/'softening' this interface, thereby supporting more efficient ion uptake. In addition, the PEO-block may

assist bulk ion transport as well. Intriguingly, despite ‘diluting’ the system with an electronically inert component (the PEO-blocks), the bulk capacitance  $C^*$  related to the charge density of the electrochemically doped polymer,<sup>28</sup> is relatively little impacted by blending. This means that blending does not significantly alter the hole concentration that can be induced by doping. Since  $\mu C^*$  is comparable across blend composition, we propose that the overall electronic property of P(3HT-co-3HHT) are largely unaffected by blending. As importantly, the time scale range, over which the source-drain current is amplified in OECTs based on blends, often in a significant fashion, is notably extended (see Figure 1b and c), opening applications of such OECTs for, e.g., monitoring biological signals of specific time scales.

To achieve the fast ion transport, leading to a relatively negligible  $\Delta V_i$  and a rather stable  $g_m$  independent of Gate-Source bias sweep rate, it seems important to use a block-copolymer rather than a PEO homopolymer. The P3HT-block helps limiting large-scale phase separation and, indeed, seems to induce partial vitrification of the active P(3HT-co-3HHT). This vitrification may be the reason that a sufficiently large fraction of P(3HT-co-3HHT) segments are available for the electrochemical doping process. This point of view is emphasized when analyzing blends of P(3HT-co-3HHT) with PEO. Contrary to the P(3HT-co-3HHT):P3HT-b-PEO systems, blends between P(3HT-co-3HHT) and the PEO homopolymer feature enthalpies for the P(3HT-co-3HHT)/P3HT and PEO-melting endotherms that decrease in a linear fashion with PEO content (Figure S5), indicating that both components can relatively freely crystallize, unhindered by the addition of the other species, as is typically observed fully phase-separated systems.

Unambiguously, our blending approach can be further exploited. For instance, vitrification and compatibilization can be manipulated by the respective block length of the ‘additive’. Block-lengths, especially of the PEO-moiety, can moreover be used to manipulate the overall mechanical properties of the system. Namely, increasing the P3HT-block size could further promote vitrification at the blurred interface between mixed conductor and ‘additive’, allowing deeper doping of the mixed-conductor. Moreover, length of the blocks of the additive, especially of the PEO-moiety, can be used to manipulate the overall mechanical properties of the system. Varying the absolute and relative size of each block, especially with respect to that of the redox active polymer, will open a versatile tool box for blend control. In addition, semiconducting blocks of higher charge-carrier mobilities may be used; or blocks that can be more readily oxidized than P3HT-moieties, rendering blending such a powerful strategy. Obviously, similar principles will also apply for systems that support electron transport, expanding the possibilities to design materials systems from the outset towards specific, desired property set.

## Author Contributions

M.B. performed most of the experiments in this work including electrochemical spectroscopy, OECT fabrication and impedance measurements; experiments on P3HT were conducted by Y.A.Y.; while T.N. and D.T. provided assistance in the experiments. O.J.D performed the synthesis of the random copolymer, O.S. and S.R. did the one of the block-copolymer under the guidance of C.B. and E.C.. L.J.R provide structural characterization, together with T.N. M.B. and T.N. prepared the manuscript. N.S. and G.H. designed the research and revised the manuscript.

## Conflicts of interest

There are no conflicts to declare

## Acknowledgements

M.B. is grateful for the financial support provided by the French ministry, MESRI. N.S. acknowledges funding via the IdEX Bordeaux program (ANR-10-IDEX-03-02) and O.D. support from Chimie Balard Cirimat Carnot Institute through the ANR program N° 16 CARN 0008-01. Y.A.Y., E.C., C.B., O.J.D., G.H. and N.S. acknowledge funding by ANR project “MAPLLE” (ANR-20-CE06-0002). This research used the CMS BM11 beamline at the National Synchrotron Light Source II, a U.S. Department of Energy (DOE) Office of Science User Facility operated for the DOE Office of Science by Brookhaven National Laboratory NY, USA. M.B is grateful for access to the EquipEx ELORPrintTec facility (ANR-10-EQPX-28-01).

## References

- Higgins, S. G.; Lo Fiego, A.; Patrick, I.; Creamer, A.; Stevens, M. M. Organic Bioelectronics: Using Highly Conjugated Polymers to Interface with Biomolecules, Cells, and Tissues in the Human Body. *Adv. Mater. Technol.* **2020**, *5* (11), 2000384. <https://doi.org/10.1002/admt.202000384>.
- Rivnay, J.; Leleux, P.; Ferro, M.; Sessolo, M.; Williamson, A.; Koutsouras, D. A.; Khodagholy, D.; Ramuz, M.; Strakosas, X.; Owens, R. M.; Benar, C.; Badier, J.-M.; Bernard, C.; Malliaras, G. G. High-Performance Transistors for Bioelectronics through Tuning of Channel Thickness. *Sci. Adv.* **2015**, *1* (4), e1400251 <https://doi.org/10.1126/sciadv.1400251>.
- Paulsen, B. D.; Tybrandt, K.; Stavrinidou, E.; Rivnay, J. Organic Mixed Ionic–electronic Conductors. *Nat. Mater.* **2020**, *19* (1), 13–26. <https://doi.org/10.1038/s41563-019-0435-z>.
- Laiho, A.; Herlogsson, L.; Forchheimer, R.; Crispin, X.; Berggren, M. Controlling the Dimensionality of Charge Transport in Organic Thin-Film Transistors. *Proc. Natl. Acad. Sci.* **2011**, *108* (37), 15069–15073. <https://doi.org/10.1073/pnas.1107063108>.
- Zeglio, E.; Eriksson, J.; Gabrielsson, R.; Solin, N.; Inganäs, O. Highly Stable Conjugated Polyelectrolytes for Water-Based Hybrid Mode Electrochemical Transistors. *Adv. Mater.* **2017**, *29* (19), 1605787. <https://doi.org/10.1002/adma.201605787>.
- Inal, S.; Rivnay, J.; Leleux, P.; Ferro, M.; Ramuz, M.; Brendel, J. C.; Schmidt, M. M.; Thelakkat, M.; Malliaras, G. G. A High Transconductance Accumulation Mode Electrochemical Transistor. *Adv. Mater.* **2014**, *26* (44), 7450–7455. <https://doi.org/10.1002/adma.201403150>.
- Giovannitti, A.; Sbircea, D.-T.; Inal, S.; Nielsen, C. B.; Bandiello, E.; Hanifi, D. A.; Sessolo, M.; Malliaras, G. G.; McCulloch, I.; Rivnay, J. Controlling the Mode of Operation of Organic Transistors through Side-Chain Engineering. *Proc. Natl. Acad. Sci.* **2016**, *113* (43), 12017–12022. <https://doi.org/10.1073/pnas.1608780113>.
- Giovannitti, A.; Nielsen, C. B.; Sbircea, D. T.; Inal, S.; Donahue, M.; Niazi, M. R.; Hanifi, D. A.; Amassian, A.; Malliaras, G. G.; Rivnay, J.; McCulloch, I. N-Type Organic Electrochemical Transistors with Stability in Water. *Nat. Commun.* **2016**, *7*, 1–9, 13066. <https://doi.org/10.1038/ncomms13066>.
- Szumaska, A. A.; Maria, I. P.; Flagg, L. Q.; Savva, A.; Surgailis, J.; Paulsen, B. D.; Moia, D.; Chen, X.; Griggs, S.; Mefford, J. T.; Rashid, R. B.; Marks, A.; Inal, S.; Ginger, D. S.; Giovannitti, A.; Nelson, J. Reversible Electrochemical Charging of N-Type Conjugated Polymer Electrodes in Aqueous Electrolytes. *J. Am. Chem. Soc.* **2021**, *143* (36), 14795–14805. <https://doi.org/10.1021/jacs.1c06713>.
- Dyson, M. J.; Lariou, E.; Martin, J.; Li, R.; Erothu, H.; Wantz, G.; Topham, P. D.; Dautel, O. J.; Hayes, S. C.; Stavrinou, P. N.; Stingelin, N. Managing Local Order in Conjugated Polymer Blends via Polarity Contrast. *Chem. Mater.* **2019**, *31* (17), 6540–6547. <https://doi.org/10.1021/acs.chemmater.8b05259>.

- (11) Venkateshvaran, D.; Nikolka, M.; Sadhanala, A.; Lemaur, V.; Zelazny, M.; Kepa, M.; Hurhangee, M.; Kronemeijer, A. J.; Pecunia, V.; Nasrallah, I.; Romanov, I.; Broch, K.; McCulloch, I.; Emin, D.; Olivier, Y.; Cornil, J.; Beljonne, D.; Sirringhaus, H. Approaching Disorder-Free Transport in High-Mobility Conjugated Polymers. *Nature* **2014**, *515* (7527), 384–388. <https://doi.org/10.1038/nature13854>.
- (12) Noriega, R.; Rivnay, J.; Vandewal, K.; Koch, F. P. V.; Stingelin, N.; Smith, P.; Toney, M. F.; Salleo, A. A General Relationship between Disorder, Aggregation and Charge Transport in Conjugated Polymers. *Nat. Mater.* **2013**, *12* (11), 1038–1044. <https://doi.org/10.1038/nmat3722>.
- (13) Moser, M.; Hidalgo, T. C.; Surgailis, J.; Gladisch, J.; Ghosh, S.; Sheelamanthula, R.; Thiburce, Q.; Giovannitti, A.; Salleo, A.; Gasparini, N.; Wadsworth, A.; Zozoulenko, I.; Berggren, M.; Stavrinidou, E.; Inal, S.; McCulloch, I. Side Chain Redistribution as a Strategy to Boost Organic Electrochemical Transistor Performance and Stability. *Adv. Mater.* **2020**, *32* (37), 2002748. <https://doi.org/10.1002/adma.202002748>.
- (14) Schmode, P.; Ohayon, D.; Reichstein, P. M.; Savva, A.; Inal, S.; Thelakkat, M. High-Performance Organic Electrochemical Transistors Based on Conjugated Polyelectrolyte Copolymers. *Chem. Mater.* **2019**, *31* (14), 5286–5295. <https://doi.org/10.1021/acs.chemmater.9b01722>.
- (15) Mai, C.-K.; Arai, T.; Liu, X.; Fronk, S. L.; Su, G. M.; Segalman, R. A.; Chabiny, M. L.; Bazan, G. C. Electrical Properties of Doped Conjugated Polyelectrolytes with Modulated Density of the Ionic Functionalities. *Chem. Commun.* **2015**, *51* (99), 17607–17610. <https://doi.org/10.1039/C5CC06690E>.
- (16) Scaccabarozzi, A. D.; Stingelin, N. Semiconducting-Insulating Polymer Blends for Optoelectronic Applications—A Review of Recent Advances. *J. Mater. Chem. A* **2014**, *2* (28), 10818–10824. <https://doi.org/10.1039/C4TA01065E>.
- (17) Yamamoto, S.; Malliaras, G. G. Controlling the Neuromorphic Behavior of Organic Electrochemical Transistors by Blending Mixed and Ion Conductors. *ACS Appl. Electron. Mater.* **2020**, *2* (7), 2224–2228. <https://doi.org/10.1021/acsaem.0c00203>.
- (18) Scaccabarozzi, A. D.; Basham, J. I.; Yu, L.; Westacott, P.; Zhang, W.; Amassian, A.; McCulloch, I.; Caironi, M.; Gundlach, D. J.; Stingelin, N. High-Density Polyethylene—an Inert Additive with Stabilizing Effects on Organic Field-Effect Transistors. *J. Mater. Chem. C* **2020**, *8* (43), 15406–15415. <https://doi.org/10.1039/D0TC03173A>.
- (19) Goffri, S.; Müller, C.; Stingelin-Stutzmann, N.; Breiby, D. W.; Radano, C. P.; Andreasen, J. W.; Thompson, R.; Janssen, R. A. J.; Nielsen, M. M.; Smith, P.; Sirringhaus, H. Multicomponent Semiconducting Polymer Systems with Low Crystallization-Induced Percolation Threshold. *Nat. Mater.* **2006**, *5* (12), 950–956. <https://doi.org/10.1038/nmat1779>.
- (20) Kumar, A.; Baklar, M. A.; Scott, K.; Kreouzis, T.; Stingelin-Stutzmann, N. Efficient, Stable Bulk Charge Transport in Crystalline/Crystalline Semiconductor-Insulator Blends. *Adv. Mater.* **2009**, *21* (44), 4447–4451. <https://doi.org/10.1002/adma.200900717>.
- (21) Ferenczi, T. A. M.; Müller, C.; Bradley, D. D. C.; Smith, P.; Nelson, J.; Stingelin, N. Organic Semiconductor:Insulator Polymer Ternary Blends for Photovoltaics. *Adv. Mater.* **2011**, *23* (35), 4093–4097. <https://doi.org/10.1002/adma.201102100>.
- (22) Pacheco-Moreno, C. M.; Schreck, M.; Scaccabarozzi, A. D.; Bourgun, P.; Wantz, G.; Stevens, M. M.; Dautel, O. J.; Stingelin, N. The Importance of Materials Design to Make Ions Flow: Toward Novel Materials Platforms for Bioelectronics Applications. *Adv. Mater.* **2017**, *29* (4), 1604446. <https://doi.org/10.1002/adma.201604446>.
- (23) Nicolini, T.; Surgailis, J.; Savva, A.; Scaccabarozzi, A. D.; Nakar, R.; Thuau, D.; Wantz, G.; Richter, L. J.; Dautel, O.; Hadziioannou, G.; Stingelin, N. A Low-Swelling Polymeric Mixed Conductor Operating in Aqueous Electrolytes. *Adv. Mater.* **2021**, *33* (2), 2005723. <https://doi.org/10.1002/adma.202005723>.
- (24) Inal, S.; Malliaras, G. G.; Rivnay, J. Benchmarking Organic Mixed Conductors for Transistors. *Nat. Commun.* **2017**, *8* (1), 1767. <https://doi.org/10.1038/s41467-017-01812-w>.
- (25) Meddings, N.; Heinrich, M.; Overney, F.; Lee, J.-S.; Ruiz, V.; Napolitano, E.; Seitz, S.; Hinds, G.; Raccichini, R.; Gaberšček, M.; Park, J. Application of Electrochemical Impedance Spectroscopy to Commercial Li-Ion Cells: A Review. *J. Power Sources* **2020**, *480*, 228742. <https://doi.org/10.1016/j.jpowsour.2020.228742>.
- (26) Zou, C.; Zhang, L.; Hu, X.; Wang, Z.; Wik, T.; Pecht, M. A Review of Fractional-Order Techniques Applied to Lithium-Ion Batteries, Lead-Acid Batteries, and Supercapacitors. *J. Power Sources* **2018**, *390* (March), 286–296. <https://doi.org/10.1016/j.jpowsour.2018.04.033>.
- (27) Amand, S.; Musiani, M.; Orazem, M. E.; Pébère, N.; Tribollet, B.; Vivier, V. Constant-Phase-Element Behavior Caused by Inhomogeneous Water Uptake in Anti-Corrosion Coatings. *Electrochim. Acta* **2013**, *87*, 693–700. <https://doi.org/10.1016/j.electacta.2012.09.061>.
- (28) Flagg, L. Q.; Bischak, C. G.; Onorato, J. W.; Rashid, R. B.; Luscombe, C. K.; Ginger, D. S. Polymer Crystallinity Controls Water Uptake in Glycol Side-Chain Polymer Organic Electrochemical Transistors. *J. Am. Chem. Soc.* **2019**, *141* (10), 4345–4354. <https://doi.org/10.1021/jacs.8b12640>.
- (29) Proctor, C. M.; Rivnay, J.; Malliaras, G. G. Understanding Volumetric Capacitance in Conducting Polymers. *J. Polym. Sci. Part B Polym. Phys.* **2016**, *54* (15), 1433–1436. <https://doi.org/10.1002/polb.24038>.
- (30) Enengl, C.; Enengl, S.; Pluczyk, S.; Havlicek, M.; Lapkowski, M.; Neugebauer, H.; Ehrenfreund, E. Doping-Induced Absorption Bands in P3HT: Polarons and Bipolarons. *ChemPhysChem* **2016**, *17* (23), 3836–3844. <https://doi.org/10.1002/cphc.201600961>.
- (31) Koklu, A.; Wustoni, S.; Guo, K.; Silva, R.; Salvigni, L.; Hama, A.; Diaz-Galicia, E.; Moser, M.; Marks, A.; McCulloch, I.; Grünberg, R.; Arold, S. T.; Inal, S. Convection Driven Ultrarapid Protein Detection via Nanobody-Functionalized Organic Electrochemical Transistors. *Adv. Mater.* **2022**, *34* (35), 2202972. <https://doi.org/10.1002/adma.202202972>.
- (32) Thomas, E. M.; Nguyen, P. H.; Jones, S. D.; Chabiny, M. L.; Segalman, R. A. Electronic, Ionic, and Mixed Conduction in Polymeric Systems. *Annu. Rev. Mater. Res.* **2021**, *51* (1), 1–20. <https://doi.org/10.1146/annurev-matsci-080619-110405>.
- (33) J. H. Kim, S. Kim, G. Kim and M. Yoon, Designing Polymeric Mixed Conductors and Their Application to Electrochemical-Transistor-Based Biosensors. *Macromol. Biosci.* **2020**, *20*, 2000211. <https://doi.org/10.1002/mabi.202000211>

## COMMUNICATION